A compact DD neutron generator–based NAA system to quantify manganese (Mn) in bone *in vivo*

Yingzi Liu[1], **Patrick Byrne**[1], **Haoyu Wang**[2], **David Koltick**[2], **Wei Zheng**[1], and **Linda H. Nie**[1]

[1]School of Health Sciences, Purdue University

[2]Physics Department, Purdue University

Abstract

A deuterium-deuterium (DD) neutron generator–based neutron activation analysis (NAA) system has been developed to quantify metals, including manganese (Mn), in bone *in vivo*. A DD neutron generator with a flux of up to $3*10^9$ neutrons/second was set up in our lab for this purpose. Optimized settings, including moderator, reflector, and shielding material and thickness, were selected based on Monte Carlo (MC) simulations conducted in our previous work. Hand phantoms doped with different Mn concentrations were irradiated using the optimized DD neutron generator irradiation system. The Mn characteristic γ-rays were collected by an HPGe detector system with 100% relative efficiency. The calibration line of the Mn/calcium (Ca) count ratio versus bone Mn concentration was obtained ($R^2 = 0.99$) using the hand phantoms. The detection limit (DL) was calculated to be about 1.05 μg/g dry bone (ppm) with an equivalent dose of 85.4 mSv to the hand. The DL can be reduced to 0.74 ppm by using two 100% HPGe detectors. The whole body effective dose delivered to the irradiated subject was calculated to be about 17 μSv. Given the average normal bone Mn concentration of 1 ppm in the general population, this system is promising for *in vivo* bone Mn quantification in humans.

1. Introduction

Manganese (Mn) is an essential trace element in the human body. Adverse health effects occur when body Mn storage is either too low or too high. Mn deficiency is generally not recognized among humans because of their diverse diets. Yet, Mn overexposure is common. Occupational exposure to Mn often takes place in mining, welding, steel industry, and other industrial settings (Crossgrove and Zheng, 2004). Environmental exposure to Mn has been reported in the uses of Mn-containing products (e.g. Mn-based pesticides), contamination in drinking water and food (Bouchard et al., 2011), and the use of Mn compounds in gasoline (Butcher et al., 1999). There are also reports of excessive Mn exposure among ephedron drug abusers (Yildirim et al., 2009).

With excessive Mn deposition, chronic Mn toxicity can be evidenced in cardiovascular, liver, reproductive, and developmental problems, although it is mainly seen to affect lung tissue and the central nervous system (Crossgrove and Zheng, 2004, Jiang and Zheng, 2005). Indeed, workers exposed to Mn have reported various neurological disorders, including poor

eye-hand coordination, reduced cognitive flexibility, tremors, and poor postural stability (Levy and Nassetta, 2003, Rodier, 1955, Wennberg et al., 1991). In severe cases, a devastating neurological impairment called "manganism" occurs (Goldhaber, 2003, Lucchini et al., 2009, Martin, 2006, Santamaria et al., 2007, Racette et al., 2012). At lower levels, Mn exposure causes more subtle neurological disorders (Kim et al., 2011, Zoni et al., 2012, Laohaudomchok et al., 2011). The symptoms of chronic Mn toxicity usually become progressive and are irreversible, reflecting permanent damage to neurological structures (Aschner et al., 2007, Jiang et al., 2006).

Mn levels in the human body have been estimated from blood, serum, urine, hair, and toenails. There is evidence that these biomarkers are useful in some ways. For instance, blood, hair, and toenail Mn concentrations were found to be higher in occupationally exposed workers than in matched controls in different studies (Myers et al., 2003, Zheng et al., 2011). However, these biomarkers are of little use for long-term cumulative exposure assessment. Analyses of whole blood Mn were found to be highly variable among human population and are not significantly correlated with Mn-induced neurotoxicity (Santos et al., 2013). This is due primarily to a short half-life of Mn in blood and large intracellular distribution (Zheng et al., 2000). High variability was also observed for Mn concentrations in toenails and hair (Wongwit et al., 2004, Bader et al., 1999). In addition hair and nail samples are subject to external contamination. Recently, MRI imaging technologies have been developed to quantify Mn in brain tissue using the signal intensity in the basal ganglia region (Dydak et al., 2011, Jiang et al., 2007). While it is advantageous to directly relate Mn exposure to brain function, this technology again has the limitation that Mn is released from the brain after a short time, and hence it only reflects recent Mn exposure. Overall, the lack of a reliable cumulative exposure biomarker limits the capacity for epidemiologic studies to detect a relationship between Mn exposure and neurodegeneration, especially for low-level exposures and their more subtle neurological effects.

On the other hand, bone has much greater potential to be a reliable biomarker for cumulative Mn in the body. Schroeder et al. (1966) reported an average Mn concentration of 2 μg/g in bone ash, which gives rise to about 32.5% of body Mn being contained in bone, according to our previous calculation (Liu et al., 2013). International Commission on Radiological Protection (ICRP) reported about 40% of body Mn in bone (ICRP, 1975). A recent study shows that the average half-life of Mn in bone is 147 days in rats that are chronically exposed to Mn-contaminated drinking water (Zheng et al., 2014), which is much longer than its half-life in other organs. The same researchers also show a significant correlation between brain Mn and bone Mn in rats fed with Mn-contained water (Hong et al., 2013). Hence, it is logical to postulate that bone is one of the main long-term storage organs for Mn in humans, and that bone Mn is a relevant and valuable biomarker for Mn neurotoxicity.

Our group has developed novel transportable neutron activation analysis (NAA) technology to quantify Mn in bone *in vivo*. In our previous work (Liu et al., 2013), the methodology and feasibility of developing such a system were investigated using Monte Carlo simulations and a deuterium-tritium (DT)–based neutron generator system. The purposes of the current study were: (1) to set up a DD-based neutron generator system; (2) to characterize, test, and optimize the system for in vivo Mn quantification using Monte Carlo simulations and

experiments; (3) to improve the system by modifying the moderator/reflector/shielding system; (4) to set up and use a 100% high efficiency HPGe detection system to measure the Mn γ-rays produced by neutron activation, and to reduce the detection limit (DL) of the system for *in vivo* bone Mn quantification.

2. Materials and methods

2.1. Monte Carlo simulation

This project used the Monte Carlo N-Particle (MCNP) code, which was developed by Los Alamos National Laboratory (LANL). MCNP code uses the Monte Carlo method to simulate the propagation of particles, including neutrons and photons (http://mcnp.lanl.gov/). To the benefit of our project, the new version of the MCNP code contains the latest cross-sectional data and is able to tally the neutron flux, activation, and radiation dose based on user-defined source/moderator/reflector/shielding geometry and composition. At thermal neutron energies, the binding of the scattering nucleus in a solid, liquid, or gas affects the cross-section and the angular and energy distributions of the scattered neutrons. When available, the S(α, β) data were included to better simulate thermal neutron interaction. This project used MCNP5 version 1.6 of the code, and all input files were checked with the VISED X_24E visual editor for geometric consistency. All the results have uncertainties of less than 5%.

2.2. DD neutron generator and neutron flux

The neutron generator used in this project was a customized DD-109 manufactured by Adelphi Technology Inc. (Redwood, CA). The main components of a DD neutron generator are the ion source, ion extractor, beam target, power supply/electronics rack, and heat exchanger. Figure 1 shows the DD neutron generator installed in our lab, while Figure 2 is a schematic plot of the generator head with dimensions provided by Adelphi. A deuterium (D_2) gas bottle was mounted beside the table to provide a continuous supply of deuterium gas when the system was operating. The gas line was highly vacuumed by a roughing pump and a more rigorous turbo pump. Like all DD neutron generators, the DD-109 employed in this study used the DD fusion reaction ($^2D + {}^2D \rightarrow {}^4He \rightarrow {}^3He + n$) and was driven by an ion beam supplied by a radio frequency–driven ion source.

The target for this project was made from titanium-coat ed copper. To maximize the neutron production and lifetime of the target, the temperature of the titanium surface was maintained by active cooling. The V-shaped target was also designed for efficient cooling, as shown in Figure 2. To shield the bremsstrahlung x-rays generated by the electrons emitted back to the plasma source from the primary ion interaction at the titanium target, 3 mm thick lead was placed around the generator head.

Neutron flux of up to 3×10^9 neutrons/second can be produced with this generator, depending on the acceleration voltage and the ion current. The voltage varies from 80 kV to 125 kV, while the current varies from 10 mA to 13 mA. The true neutron flux can be determined by a lightweight NSN3 neutron survey meter (Fuji Electric Corp.) coupled with MC simulation results. This neutron survey meter uses mixed methane and nitrogen gas to measure fast neutrons based on elastic scattering reactions and thermal neutrons based

on ^{14}N(n,p) reactions. The neutron ambient dose equivalent can then be obtained, taking into account the ICRP 74 (ICRP, 1997) neutron flux-to-dose equivalent rate conversion factors (Nunomiya et al., 2011). The NSN3 dosimeter's mono-energetic and continuous energy response is within 50% difference from thermal to 15 MeV neutrons.

2.3. Moderator/reflector/shielding system and experimental setup of the DD neutron generator

Based on the MC simulation results presented for our past work (Liu et al., 2013), an optimized moderator/reflector/shielding system was built to create a cavity for the irradiation of human hands. Our previous paper showed that an optimized configuration consists of 5 cm of paraffin as the moderator and >10 cm of paraffin as the reflector. In the system used in the current study, polyethylene was used instead of paraffin because paraffin is flammable. This will not significantly impact the results, however, since the composition of paraffin and polyethylene are similar, as shown in our paper cited above. Specifically, 5 cm of polyethylene was used as the moderator; 10 cm of polyethylene was used as the reflector; and the shielding structure was made of >30 cm of polyethylene. The neutron dose outside of the shielding was measured to be 2–5 mR/hour based on this configuration. Figure 3 shows the experimental setup of the DD neutron generator with the polyethylene moderator/reflector/shielding system, with part of the shielding removed to present a better view of the human hand cavity.

Work is in progress to build a more compact shielding structure with a tighter fit around the generator head except on the side where the hand will be irradiated. Our most recent experimental and simulation results (not presented in this paper) also show that the neutron spectra are significantly altered as the size of the gaps between the moderator blocks and reflector blocks changes. In addition, graphite has been demonstrated to be a more efficient material for a reflector. More work continues to be conducted to further optimize this moderator and reflector configuration.

2.4. Manganese-doped human hand phantoms

Five Mn-doped hand phantoms were manufactured and used in this study. The Mn concentrations in the phantoms were 0, 5, 10, 15, and 20 μg Mn/g bone (which corresponds to 0, 22, 44, 66, and 88μg Mn/g Ca). Other elements in bone that might interfere with the spectrum through neutron activation were also added to the phantoms to better simulate real human hands. The concentration of each element in the bones of the hand was calculated based on ICRP publication 23's gross and element content of the cortical bone of a reference human male (ICRP, 1975). Table 1 lists all the elements included and the weight of their chemical compounds.

All the chemical compounds were first diluted in distilled water before being added to the matrix to ensure a better homogeneity of the elements in the phantoms. The phantoms were then dried in the hood for one day. These phantoms were bone-equivalent phantoms, but they did not have the shape of a human hand. More work is in progress to manufacture hand-shaped phantoms encased in soft tissue.

2.5. *In vivo* neutron activation analysis

With the system shown in Figure 3, Mn concentrations present in the hand bone of a human subject can be noninvasively determined using *in vivo* neutron activation analysis (IVNAA). As described in our previous paper (Liu et al., 2013), during neutron activation, characteristic γ-rays are produced following the radioactive decay of the product from an $^AX(n,\gamma)^{(A+1)}X$ nuclear reaction. By collecting the characteristic γ-rays and calculating their total counts, the concentration of the element of interest can be determined. For Mn quantification, neutrons interact with ^{55}Mn and produce ^{56}Mn with a thermal neutron capture cross section of 13.3 barns. Unstable ^{56}Mn atoms decay to ^{56}Fe, which emits 847 keV characteristic γ-rays. These γ-rays can then be collected by a γ-ray detection system. ^{56}Mn's relatively long half-life of 2.58 hours allows for delayed γ counting. The calculation for the intensity of the characteristic γ-rays can be found in our previous paper.

Using the fm4 card in MCNP5, the probability of the activated nucleus can be obtained. Together with the activation equation, the simulated total γ-ray counts can be expressed as:

$$C_{Total} = N \times \gamma \times \varepsilon \times S \times D \times C \quad (1)$$

where C_{Total} is the γ-ray counts that will be measured by the γ-ray detector; N is the total activated ^{56}Mn number from the simulation result; γ is the branch ratio of the γ-rays; ε is the absolute detection efficiency; $S(= 1 - e^{-\lambda t_i})$ is the saturation factor with t_i representing irradiation time; $D(= e^{-\lambda t_d})$ is the decay factor with t_d representing decay time; and $C(=1 - e^{-\lambda t_c})/\lambda$ is the counting factor with t_c representing counting time. C_{Total} can be compared to experiment results to test the consistency of the simulation and experimental results.

The irradiation, decay, and counting time can also be optimized to determine the best time sequence. We selected 10 minutes of irradiation time to allow for an acceptable dose to the hand; 5 minutes of decay time to collect a spectrum for calcium (Ca); and 30 minutes of measurement time in consideration of the time that a human subject could be expected to sit relatively still to take the measurement. This time sequence can be further improved in future work.

A sample of pure gold (Au) foil and an Mn-doped hand phantom were irradiated by the DD–based neutron generator system and then measured by an HPGe γ-ray detection system. The same scenarios were also simulated using the MC simulation model. The results from the MC simulations and the experiments were then compared. This is to validate the results from MC simulations.

2.6. HPGe detector and gamma spectrum analysis

A high-efficiency HPGe detector was used in this study for γ-ray detection. It is a model GMX90P4-ST HPGe detector with a relative efficiency of 100%. The detector is cooled by an electromechanical cooler (Ortec, Oak Ridge, TN). Lead bricks were mounted around the detector to reduce the background signal. The DSPEC Plus digital box was used for signal processing, and Maestro γ-ray spectroscopy software was used for signal collection. The efficiency of the system was calibrated using a multi-radionuclide calibration source with known activities. The efficiency equation was obtained as: efficiency $=1.0548 \times$

$energy(keV)^{-0.688}$ at 5 cm away from the detector's window. Figure 4 shows two high-efficiency detectors with a possible configuration of how a hand could be measured. Notably, only one of these detectors was used in this project because the other one was experiencing some technical problems.

Gamma-ray spectrum analysis was performed using an in-house fitting procedure programmed in the commercial software package IGOR Pro 6 (Wave Metrics, Inc., Lake Oswego, OR). The γ-ray peaks were fitted using the Gaussian function for net counts and an exponential function to account for background.

2.7. System calibration and the Mn/Ca ratio

The most straightforward way to calibrate the system for Mn quantification is to build a calibration line of ^{56}Mn γ-ray counts versus Mn concentration. However, this count would be affected by the thermalization of the neutrons within the samples, the thickness of the soft tissue in the hand, the weight of the hand, and the slightly different irradiation geometries. To account for these differences, Mn γ-ray counts can be normalized to Ca γ-ray counts, since the concentration of Ca is relatively constant in bone. Thus, a calibration line representing the Mn/Ca ratio versus Mn concentration was established.

3. Results

3.1. Neutron flux

As described above, neutron flux can be determined using a neutron generator coupled with MC simulation results. Figure 5 shows a cross-sectional plot of the neutron activation system used in the MC simulation model. To produce approximately 10^9 neutrons per second, the magnetron was set to 5 kV and 80 mA; the accelerator was set to 120 kV and 16 mA; and the D_2 gas flow was set to 1.2 standard cubic centimeters per minute (SCCM) with a pressure of ~5.0 mTorr (~4.7 mTorr in operation). The neutron dose, as measured from one side by the NSN3 dosimeter when the shielding was open, was 948.6 mRem/h at 109 cm away from the neutron source. The NSN3 neutron survey meter measures ambient neutron dose equivalent H*(10), so ICRP-74 (ICRP, 1997) neutron flux-to-dose equivalent rate conversion factors were employed in MCNP5 input files to obtain a dose measure that equaled the ambient dose equivalent. The simulated neutron dose for the neutron flux of 1×10^9 neutrons/second at the 109 cm was 1374.5 mRem/h. Given the measured dose of 948.6 mRem/h at the same spot, the actual neutron flux was calculated to be about 7×10^8 neutrons/second.

3.2. Neutron activation using MC simulations and experiments

With the parameters and settings described above, and in order to assess how the MC simulation results compared to experimental results, a 0.121 gram sample of Au foil was irradiated in the irradiation cavity for 10 minutes, decayed for 2 hours, and measured for 1 hour with the HPGe γ-ray detection system. Additionally, a 20 ppm Mn-doped hand phantom was also irradiated in the irradiation cavity for 10 minutes, decayed for 10 minutes, and measured for 30 minutes with the HPGe detection system.

The Au γ-ray counts calculated from the experiment was 818.2±27.6, compared to the simulation result of 809.4±1.1. The Mn γ-ray counts calculated from the experiment, based on the net peak counts from the spectrum analysis was 238.8±24.8, compared to the simulation result of 141.2±0.2 taking into account the detector efficiency. Several factors might have contributed to the discrepancy for Mn measurement and simulation, with the main factor to be the difficulty to determine the detector efficiency for the measurement of the hand phantom (in contrast, it is much easier to obtain an accurate detector efficiency for the measurement of Au foil); these factors are considered in the discussion section.

3.3. Data collection, Mn spectrum, Mg interference, and the detection limit

Mn-doped hand phantoms with Mn concentrations of 0, 5, 10, 15, and 20 ppm were placed in the sample cavity and irradiated for 10 minutes, decayed for 5 minutes, and measured by the HPGe detector for 30 minutes. The spectrum collected from the 5 ppm phantom is illustrated in Figure 6. With an energy resolution of 2.0 keV at 1.33 MeV, the peak of Mn γ-ray at 847 keV can be clearly seen. The background in that energy range is mainly from Compton scattering and is relatively low. An enlarged Mn peak is shown at the top right of the figure. A magnesium (Mg) γ-ray peak at 844 keV is also observed from the spectrum. Although the Mg concentration in the hand phantoms is much greater than the Mn concentration, as shown in Table 1, the interference of the Mg γ-ray peak is minimal, even with a Mn concentration at as low as 5 ppm, as shown in Figure 6.

The detection limit (DL) of the system was calculated based on the measurements taken from the Mn-doped phantoms. It was calculated using the following formula:

$$DL = \frac{2 \times \sqrt{background}}{C} \quad (2)$$

where background is the background counts under the Mn γ-ray peak for the 0 ppm phantom, and C (counts/ppm) is the slope of the regression line of Mn counts versus Mn concentration. The energy range of the background was estimated to be 4 sigma of the Mn γ-ray Gaussian peak, which covers 96% of the peak counts. Sigma was estimated from the fitting program built into IGOR. The DL calculated from equation 2 was 1.05 ppm.

3.4. Bone Mn calibration line

The spectra for all the Mn-doped hand phantoms (0, 5, 10, 15, and 20 ppm) were analyzed. The net peak counts for Mn and Ca were calculated using our in-house peak fitting program. The Mn/Ca ratio versus Mn concentration was then plotted, as shown in Figure 7. The R-square for the correlation was 0.99, which indicates that the phantoms are a good configuration and that the calibration procedure works.

3.5. Radiation dose

The radiation dose to a human hand was calculated using MC simulations. After 10 minutes of irradiation at a neutron flux of 7×10^8 neutrons/second, the equivalent dose to a hand was found to be 85.4 mSv. The dose outside of the shielding was calculated using MC simulations and measured using the NSN3 neutron meter. The simulated dose rate was 3.88

mRem/hour or 38.8 μSv/hour with the neutron flux of 7×10^8 neutrons/second, which gives rise to a dose of about 6.5 μSv for 10 minutes of irradiation. The measured dose rate was about 3.85 mRem/hour or 38.5 μSv/hour, which is very close to the simulated value. The weight of a human hand accounted for about 1.25% of the weight of the whole body. The tissue weighting factor for the more sensitive organs in hand, skin and bone surface, is 0.01. Taking into account the tissue weighting factor, the whole body effective dose was calculated to be $85.4 \times 10^3 \times 0.01 \times 0.0125 + 6.5 = 17$ μSv. For comparison, the whole body effective dose from a standard AP chest x-ray is about 100 μSv. The neutron spectrum inside the hand irradiation cavity is complex, and work is being conducted to obtain an accurate neutron dose inside the hand cavity using experiments to validate the hand dose calculated by simulation.

4. Discussion and future work

In this project, the neutron yield was calculated based on MC simulations and NSN3 neutron detector results. From the previous work of Nunominya et al. (2011), we can confirm that this neutron detector is accurate at measuring dose from neutrons with energy ranging from 400 keV to 10 MeV, but can largely underestimate the neutron dose from 8 keV to 250 keV. With one side of the shielding open, the major contributor of the neutron dose was from 2.45 MeV neutrons (accounting for over 90% of the total neutron spectrum, as per the simulation). It was thus concluded that the detector responded correctly to the neutron field, and that the neutron flux of 7×10^8 neutrons/second should be very close to the true flux in the setting we used.

The counts of Au γ-rays obtained from the MC simulation and from the experiment are the same within the error, while the counts of Mn γ-rays obtained from the MC simulation and from the experiment differed by a factor of 1.7. This discrepancy could have resulted from difference between the Au and Mn samples. Au sample is a foil, while Mn sample is a rectangular shaped bone equivalent phantom. We were not able to find a standard source with the same shape as the Mn-doped hand phantom and hence the detector efficiency could easily make a difference of a factor of 2. However, this should not affect the calculations of the detection limit or the calibration line, because the detector efficiency was not required in these calculations. However, more work will be done to obtain a more accurate detector efficiency curve for the Mn-doped phantoms.

Our work confirmed that a compact DD neutron generator–based NAA system can be used for the noninvasive quantification of Mn in bone *in vivo*. The detection limit was calculated to be 1.05 ppm, which is comparable to the level of Mn in the general population. With the parameters we used, the hand equivalent dose for 10 minutes of irradiation at the neutron flux of 7×10^8 neutrons/second was calculated to be 85.4 mSv. To comply with the ALARA principle, a hand equivalent dose of less than 50 mSv is desirable. By scaling down the irradiation time from 10 minutes to 5.85 minutes, the hand dose can be reduced to 50 mSv, although the DL would thereby increase by a factor of 1.7 to 1.79 ppm. However, several improvements can also be made to lower the DL. First, the moderator/reflector/shielding system can be further improved to generate more thermal neutrons within the acceptable dose range. Second, an additional high-efficiency HPGe detector can be used to cover a

better geometry of γ-ray detection; specifically, the use of two HPGe detectors (as shown in Figure 4) would reduce the DL to 1.27 ppm with 5.85 minutes of irradiation time, or to 0.74 ppm with 10 minutes of irradiation time. Third, the irradiation, decay, and measurement time can be further optimized.

Work has been conducted by other groups using a laboratory-based accelerator to quantify metals in bone *in vivo* (Aslam et al., 2009, Pejovic-Milic et al., 2009). The main advantage of our system is that it utilizes a compact DD neutron generator, which greatly reduces the necessary space and resulting complications that come with using a large accelerator. Considering that the eventual goal of developing this technology is to use it in human studies, the transportability of our system makes it a more practical approach.

Our next step is to validate the technology using a human study population and to use the data collected by the system to investigate the association between cumulative Mn exposures and various health outcomes. Other future work includes optimizing and validating the system for the *in vivo* quantification of other elements. Elements with a relatively high thermal neutron capture cross-section are the most promising for our application, although elements that accumulate in relatively high concentrations in the human body can also be considered.

5. Conclusion

A compact DD neutron generator-based NAA system has been set up in our laboratory based on our previous feasibility study. The present work shows that the system is capable of quantifying Mn in hand bone with a detection limit of 0.74 ppm when using two 100% high-efficiency HPGe detectors. To achieve this sensitivity, the hand would need to be irradiated at a neutron flux of 7×10^8 neutrons/second for 10 minutes, which would give rise to an equivalent hand dose of 85.4 mSv and a whole body effective dose of 17 μSv. This system is now ready to be tested in a human study to quantify Mn in bone for cumulative Mn exposure assessment.

Acknowledgments

References

ASCHNER M, GUILARTE TR, SCHNEIDER JS, ZHENG W. Manganese: recent advances in understanding its transport and neurotoxicity. Toxicol Appl Pharmacol. 2007; 221:131–47. [PubMed: 17466353]

ASLAM, CHETTLE DR, PEJOVIC-MILIC A, WAKER AJ. Opportunities to improve the in vivo measurement of manganese in human hands. Phys Med Biol. 2009; 54:17–28. [PubMed: 19060358]

BADER M, DIETZ MC, IHRIG A, TRIEBIG G. Biomonitoring of manganese in blood, urine and axillary hair following low-dose exposure during the manufacture of dry cell batteries. Int Arch Occup Environ Health. 1999; 72:521–7. [PubMed: 10592004]

BOUCHARD MF, SAUVE S, BARBEAU B, LEGRAND M, BRODEUR ME, BOUFFARD T, LIMOGES E, BELLINGER DC, MERGLER D. Intellectual impairment in school-age children

exposed to manganese from drinking water. Environ Health Perspect. 2011; 119:138–43. [PubMed: 20855239]

BUTCHER DJ, ZYBIN A, BOLSHOV MA, NIEMAX K. Speciation of methylcyclopentadienyl manganese tricarbonyl by high-performance liquid chromatography-diode laser atomic absorption spectrometry. Anal Chem. 1999; 71:5379–85. [PubMed: 21662735]

CROSSGROVE J, ZHENG W. Manganese toxicity upon overexposure. NMR Biomed. 2004; 17:544–53. [PubMed: 15617053]

DYDAK U, JIANG YM, LONG LL, ZHU H, CHEN J, LI WM, EDDEN RA, HU S, FU X, LONG Z, MO XA, MEIER D, HAREZLAK J, ASCHNER M, MURDOCH JB, ZHENG W. In vivo measurement of brain GABA concentrations by magnetic resonance spectroscopy in smelters occupationally exposed to manganese. Environ Health Perspect. 2011; 119:219–24. [PubMed: 20876035]

GOLDHABER SB. Trace element risk assessment: essentiality vs. toxicity. Regul Toxicol Pharmacol. 2003; 38:232–42. [PubMed: 14550763]

HONG L, O'NEAL S, NIE LH, ZHENG W. Bone Manganese (Mn) Concentrations in Sprague-Dawley Rats Following Subchronic Manganese Exposure. The Toxicologist, Society of Toxicology (SOT) 2013 annual meeting abstract. 2013:396.

ICRP. Report of the task group on reference man. International Commission on Radiological Protection; New York: 1975. Publication No.23

ICRP. Advice on the implications of the conversion coefficients for external radiations published in ICRP Publication 74 and in ICRU report 57. Memorandum from the British Committee on Radiation Units and Measurements. Br J Radiol. 1997; 70:1270–3. [PubMed: 9505846]

JIANG Y, ZHENG W. Cardiovascular toxicities upon manganese exposure. Cardiovasc Toxicol. 2005; 5:345–54. [PubMed: 16382172]

JIANG Y, ZHENG W, LONG L, ZHAO W, LI X, MO X, LU J, FU X, LI W, LIU S, LONG Q, HUANG J, PIRA E. Brain magnetic resonance imaging and manganese concentrations in red blood cells of smelting workers: search for biomarkers of manganese exposure. Neurotoxicology. 2007; 28:126–35. [PubMed: 16978697]

JIANG YM, MO XA, DU FQ, FU X, ZHU XY, GAO HY, XIE JL, LIAO FL, PIRA E, ZHENG W. Effective treatment of manganese-induced occupational Parkinsonism with p-aminosalicylic acid: a case of 17-year follow-up study. J Occup Environ Med. 2006; 48:644–9. [PubMed: 16766929]

KIM Y, BOWLER RM, ABDELOUAHAB N, HARRIS M, GOCHEVA V, ROELS HA. Motor function in adults of an Ohio community with environmental manganese exposure. Neurotoxicology. 2011; 32:606–14. [PubMed: 21840336]

LAOHAUDOMCHOK W, LIN X, HERRICK RF, FANG SC, CAVALLARI JM, SHRAIRMAN R, LANDAU A, CHRISTIANI DC, WEISSKOPF MG. Neuropsychological effects of low-level manganese exposure in welders. Neurotoxicology. 2011; 32:171–9. [PubMed: 21192973]

LEVY BS, NASSETTA WJ. Neurologic effects of manganese in humans: a review. Int J Occup Environ Health. 2003; 9:153–63. [PubMed: 12848244]

LIU Y, KOLTICK D, BYRNE P, WANG H, ZHENG W, NIE LH. Development of a transportable neutron activation analysis system to quantify manganese in bone in vivo: feasibility and methodology. Physiol Meas. 2013; 34:1593–609. [PubMed: 24165395]

LUCCHINI RG, MARTIN CJ, DONEY BC. From manganism to manganese-induced parkinsonism: a conceptual model based on the evolution of exposure. Neuromolecular Med. 2009; 11:311–21. [PubMed: 20012385]

MARTIN CJ. Manganese neurotoxicity: connecting the dots along the continuum of dysfunction. Neurotoxicology. 2006; 27:347–9. [PubMed: 16337002]

MYERS JE, THOMPSON ML, NAIK I, THEODOROU P, ESSWEIN E, TASSELL H, DAYA A, RENTON K, SPIES A, PAICKER J, YOUNG T, JEEBHAY M, RAMUSHU S, LONDON L, REES DJ. The utility of biological monitoring for manganese in ferroalloy smelter workers in South Africa. Neurotoxicology. 2003; 24:875–83. [PubMed: 14637382]

NUNOMIYA T, NAKAMURA T, KOYAMA T, INUI D, ISHIKURA T. Development of a light-weight portable neutron survey meter. Radiat Prot Dosimetry. 2011; 146:84–7. [PubMed: 21636558]

PEJOVIC-MILIC A, CHETTLE DR, OUDYK J, PYSKLYWEC MW, HAINES T. Bone manganese as a biomarker of manganese exposure: a feasibility study. Am J Ind Med. 2009; 52:742–50. [PubMed: 19753565]

RACETTE BA, CRISWELL SR, LUNDIN JI, HOBSON A, SEIXAS N, KOTZBAUER PT, EVANOFF BA, PERLMUTTER JS, ZHANG J, SHEPPARD L, CHECKOWAY H. Increased risk of parkinsonism associated with welding exposure. Neurotoxicology. 2012; 33:1356–61. [PubMed: 22975422]

RODIER J. Manganese poisoning in Moroccan miners. Br J Ind Med. 1955; 12:21–35. [PubMed: 14351643]

SANTAMARIA AB, CUSHING CA, ANTONINI JM, FINLEY BL, MOWAT FS. State-of-the-science review: Does manganese exposure during welding pose a neurological risk? J Toxicol Environ Health B Crit Rev. 2007; 10:417–65. [PubMed: 17710609]

SANTOS D, BATOREU C, MATEUS L, MARREILHA DOS SANTOS AP, ASCHNER M. Manganese in human parenteral nutrition: Considerations for toxicity and biomonitoring. Neurotoxicology. 2013

SCHROEDER HA, BALASSA JJ, TIPTON IH. Essential trace metals in man: manganese. A study in homeostasis. J Chronic Dis. 1966; 19:545–71. [PubMed: 5338081]

WENNBERG A, IREGREN A, STRUWE G, CIZINSKY G, HAGMAN M, JOHANSSON L. Manganese exposure in steel smelters a health hazard to the nervous system. Scand J Work Environ Health. 1991; 17:255–62. [PubMed: 1925437]

WONGWIT W, KAEWKUNGWAL J, CHANTACHUM Y, VISESMANEE V. Comparison of biological specimens for manganese determination among highly exposed welders. Southeast Asian J Trop Med Public Health. 2004; 35:764–9. [PubMed: 15689101]

YILDIRIM EA, ESSIZOGLU A, KOKSAL A, DOGU B, BAYBAS S, GOKALP P. Chronic manganese intoxication due to methcathinone (ephedron) abuse: a case report. Turk Psikiyatri Derg. 2009; 20:294–8. [PubMed: 19757228]

ZHENG W, FU SX, DYDAK U, COWAN DM. Biomarkers of manganese intoxication. Neurotoxicology. 2011; 32:1–8. [PubMed: 20946915]

ZHENG W, KIM H, ZHAO Q. Comparative toxicokinetics of manganese chloride and methylcyclopentadienyl manganese tricarbonyl (MMT) in Sprague-Dawley rats. Toxicol Sci. 2000; 54:295–301. [PubMed: 10774811]

ZHENG, W.; O'NEAL, SL.; HONG, L.; JONES, A. Half-life of Manganese (Mn) in Murine Bone following Oral Exposure. SOT Annual Meeting Proceeding; 2014.

ZONI S, BONETTI G, LUCCHINI R. Olfactory functions at the intersection between environmental exposure to manganese and Parkinsonism. J Trace Elem Med Biol. 2012; 26:179–82. [PubMed: 22664337]
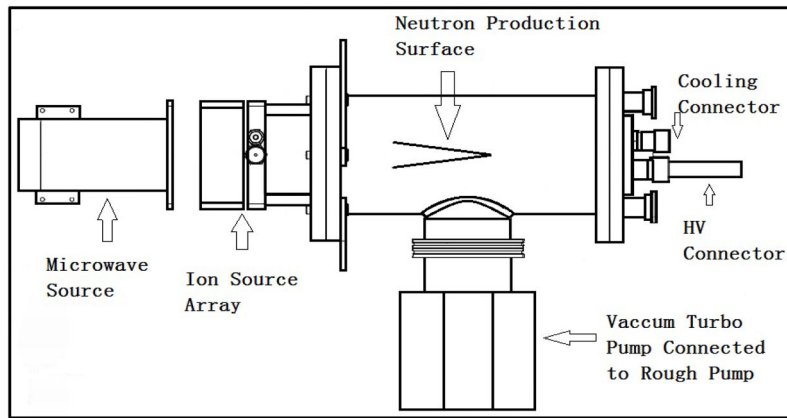
Figure 1.
DD neutron generator

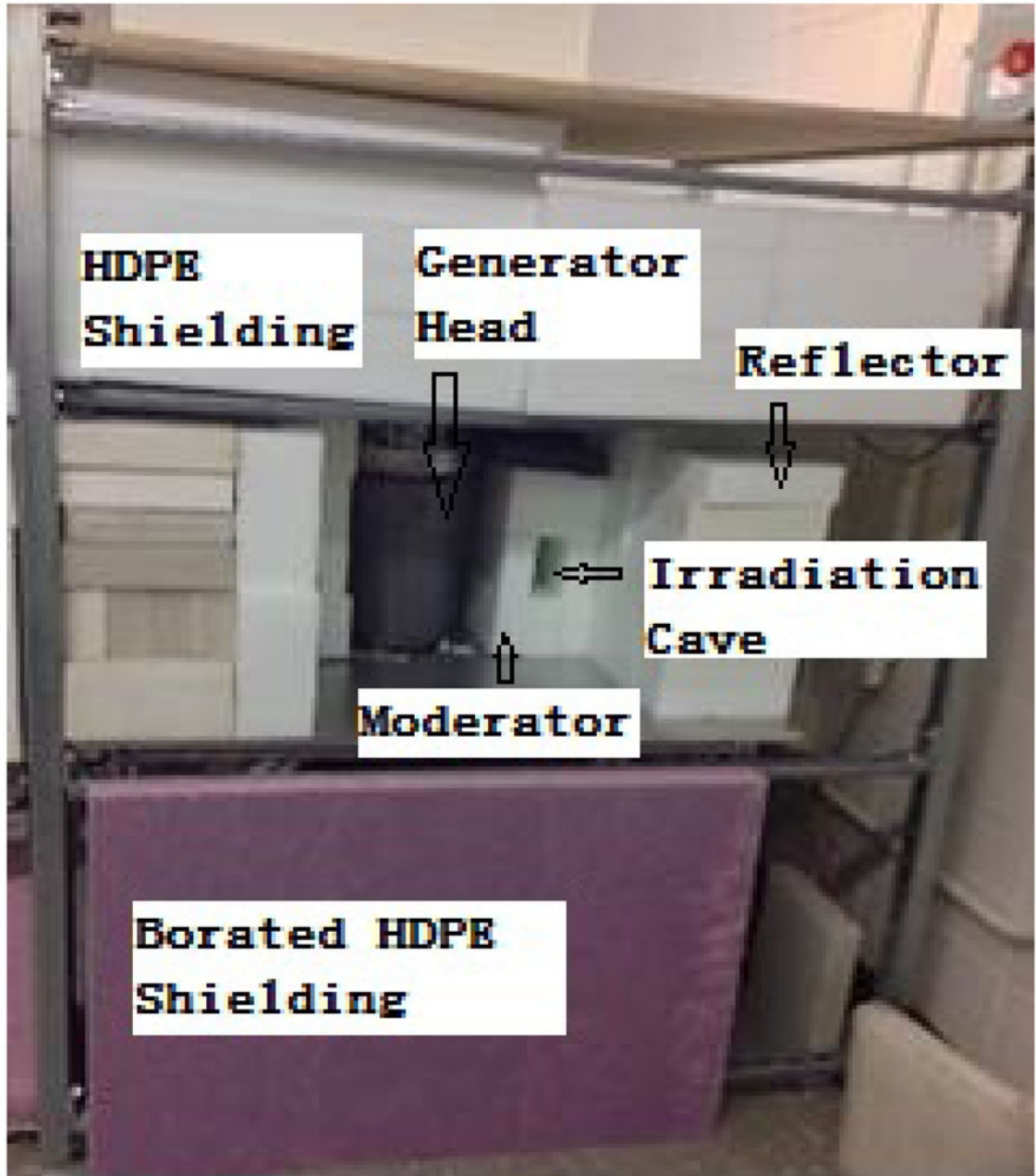**Figure 2.**
Schematic plot of DD neutron generator head

Figure 3.
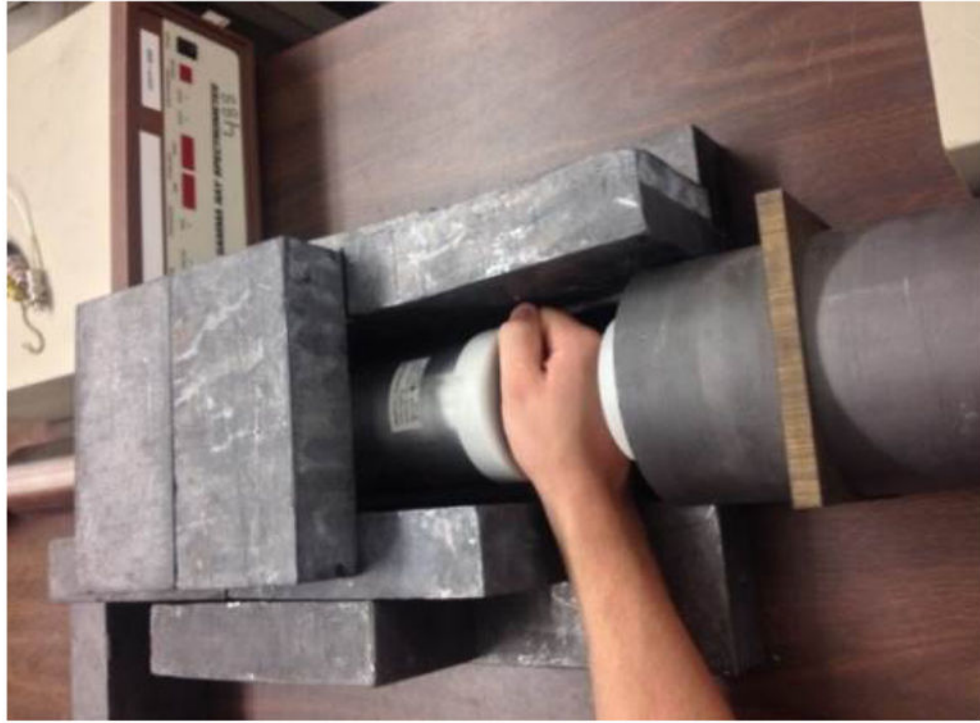Neutron activation analysis system with moderator/reflector/shielding

Figure 4.
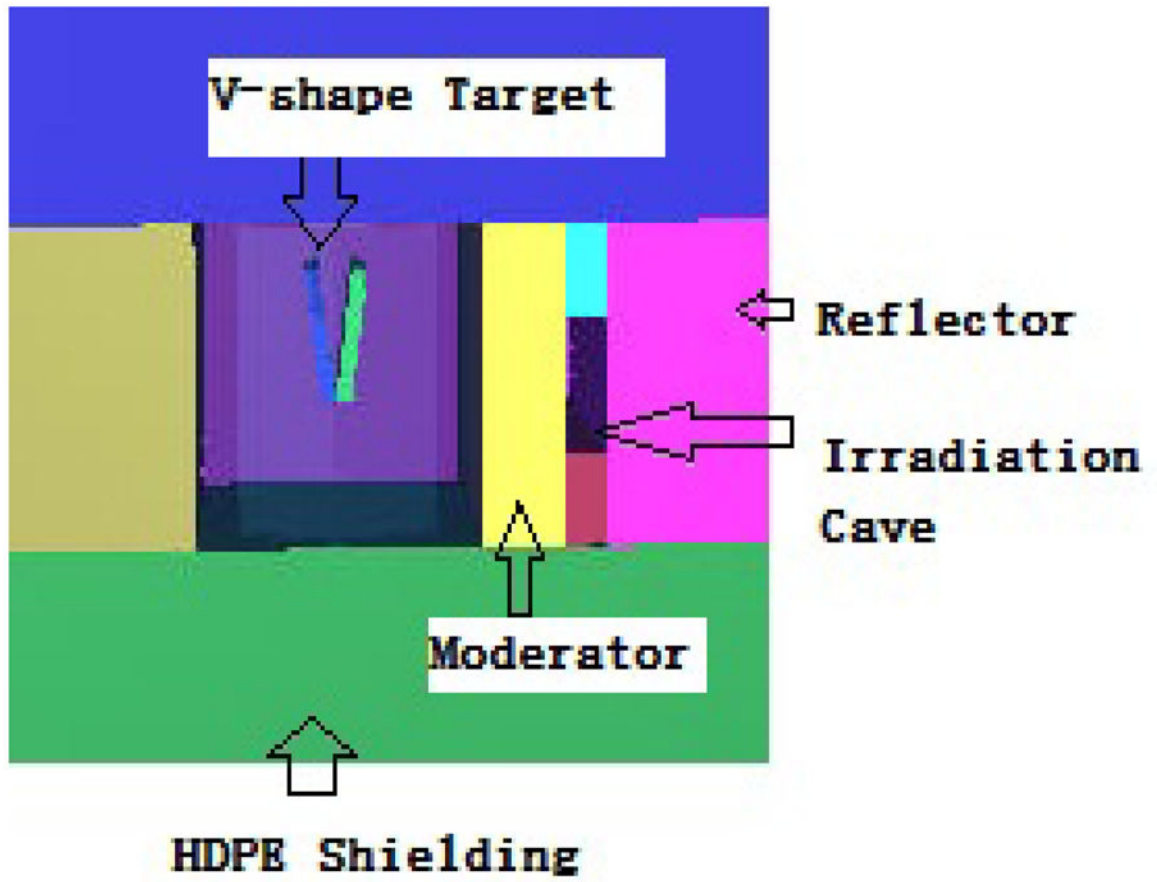High-efficiency HPGe detectors

Figure 5.
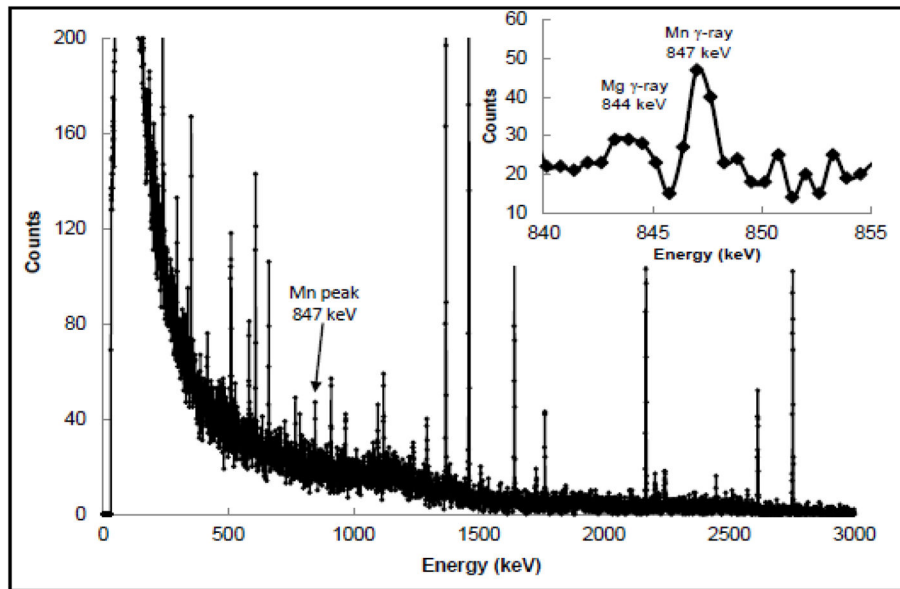Cross-sectional plot of the NAA system in the MC simulation model

Figure 6.
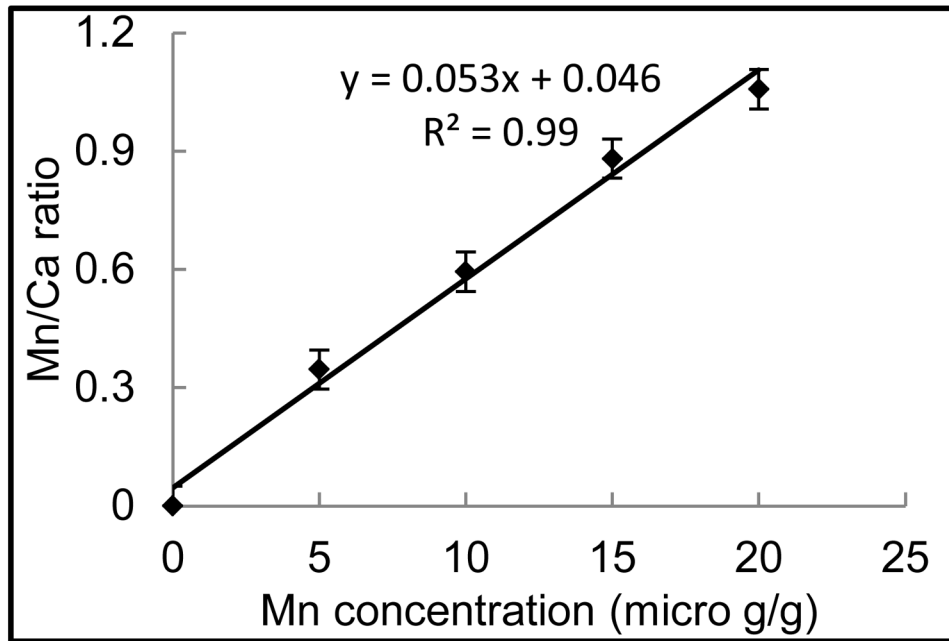Gamma-ray spectrum of a bone-equivalent phantom doped with 5 ppm Mn

Figure 7.
Mn/Ca versus Mn concentration

Table 1

Mass of each element and compound used in the hand phantoms

	Ca	Cl	Na	Mg	Mn
Reaction	$^{48}Ca(n, \gamma)^{49}Ca$	$^{37}Cl(n, \gamma)^{38}Cl$	$^{23}Na(n, \gamma)^{24}Na$	$^{26}Mg(n, \gamma)^{27}Mg$	$^{55}Mn(n, \gamma)^{56}Mn$
Mass	13.925 g	1.205 g	1.29 g	242 mg	0, 5, 10, 15, 20, ppm
Compound added	$CaSO_4$	NH_4Cl	$NaNO_3$	$MgSO_4$	$Mn(NO_3)_2$
Mass	50.4 g	1.82 g	4.77 g	1.2 g	0, 1.1, 2.2, 3.3, 4.5 mg